



Implications of a nonlinear $^{40}\text{Ar}/^{39}\text{Ar}$ age progression along the Louisville seamount trail for models of fixed and moving hot spots

Anthony A. P. Koppers

Institute of Geophysics and Planetary Physics, Scripps Institution of Oceanography, University of California, San Diego, La Jolla, CA 92093-0225, USA (akoppers@ucsd.edu)

Robert A. Duncan

College of Oceanic and Atmospheric Sciences, Oregon State University, 104 Ocean Administration Building, Corvallis, OR 97331-5503, USA (rduncan@coas.oregonstate.edu)

Bernhard Steinberger

IFREE, Japan Agency for Marine-Earth Science and Technology (JAMSTEC), 2-15 Natsushima-cho, Yokosuka-shi, Kanagawa 237-0061, Japan

[1] The Louisville seamount trail has been recognized as one of the key examples of hot spot volcanism, comparable to the classic volcanic Hawaiian-Emperor lineaments. The published total fusion $^{40}\text{Ar}/^{39}\text{Ar}$ data of *Watts et al.* [1988] showed an astonishing linear age progression, firmly establishing Louisville as a fixed hot spot in the South Pacific mantle. We report new $^{40}\text{Ar}/^{39}\text{Ar}$ ages based on high-resolution incremental heating $^{40}\text{Ar}/^{39}\text{Ar}$ dating for the same group of samples, showing a marked increase in both precision and accuracy. One of the key findings in our reexamination is that the age progression is not linear after all. The new data show a significantly decreased “apparent” plate velocity for the Louisville seamount trail older than 62 Ma but confirm the linear trend between 47 Ma and the present day (although based on only three samples over 2150 km). The most recent volcanic activity in the Louisville seamount trail has now been dated at 1.11 ± 0.04 Ma for the most southeastern seamount located at $50^{\circ}26'S$ and $139^{\circ}09'W$. These results indicate that the Louisville age progression should be interpreted on the basis of both plate and hot spot motion. In this paper we examine our new results in conjunction with the numerical mantle flow models of *Steinberger et al.* [2004] that also predict marked deviations from simple linear age progressions. With these models we can achieve a good fit to the geometry of both the Hawaiian and Louisville seamount trails and their age progressions as well as the $\sim 15^{\circ}$ paleolatitudinal shift observed by *Tarduno et al.* [2003] for the Hawaiian hot spot between 80 and 47 Ma. If the model is restricted to Pacific hot spots only, we can improve the fit to the nonlinear age trend for the Louisville seamount trail by allowing an additional rotation change of the Pacific plate around 62 Ma and by decreasing the initiation age of the Louisville plume from 120 to 90 Ma. This improved model features a significant eastward hot spot motion of $\sim 5^{\circ}$ between 80 and 30 Ma for the Louisville hot spot, which is quite dissimilar to the southward motion of the Hawaiian hot spot during the same time interval, followed by a minor $\sim 2^{\circ}$ latitudinal shift over the last 30 Myr. If hot spot tracks are considered globally, the age trend observed for the oldest part of the Louisville seamount trail does not entirely follow the numerical model predictions. This may indicate some remaining inaccuracies in the global plate circuit, but it may also indicate that the Louisville hot spot experienced a motion somewhat different than in the numerical model: faster in the interval between 62 and 47 Ma but slower before that.

Components: 9040 words, 6 figures, 4 tables.

Keywords: $^{40}\text{Ar}/^{39}\text{Ar}$ geochronology; seamounts; guyots; submarine alteration; Pacific plate; hot spots.

Index Terms: 1035 Geochemistry: Geochronology; 3040 Marine Geology and Geophysics: Plate tectonics (8150, 8155, 8157, 8158); 8121 Tectonophysics: Dynamics, convection currents and mantle plumes.

Received 3 December 2003; **Revised** 8 April 2004; **Accepted** 30 April 2004; **Published** 19 June 2004.

Koppers, A. A. P., R. A. Duncan, and B. Steinberger (2004), Implications of a nonlinear $^{40}\text{Ar}/^{39}\text{Ar}$ age progression along the Louisville seamount trail for models of fixed and moving hot spots, *Geochem. Geophys. Geosyst.*, 5, Q06L02, doi:10.1029/2003GC000671.

Theme: Movement, Dynamics, and Geochemical Evolution of the Hawaiian Hot Spot

Guest Editors: R. Duncan, J. A. Tarduno, D. Scholl, and T. Davies

1. Introduction

[2] The Louisville seamount trail (Figure 1) is a 4300 km long chain of submarine volcanoes that are inferred to have been built in the past 80 Myr as the Pacific plate moved over a persistent melt anomaly or hot spot [Hawkins *et al.*, 1987; Lonsdale, 1988]. The Louisville hot spot is considered the South Pacific counterpart of the much better studied Hawaiian hot spot and represents one of only three primary hot spots in the Pacific basin [Courtilot *et al.*, 2003]. Recent ocean drilling in the Emperor Seamounts, followed by paleomagnetic analyses of cored samples, has documented a substantial $\sim 15^\circ$ southward motion of the Hawaiian hot spot prior to 47 Ma [Tarduno *et al.*, 2003] and, as a result, calls into question whether Pacific hot spots constitute a fixed reference frame in the Earth's deep mantle. One end-member model advocates that the primary hot spots moved in concert and would comprise a relatively fixed or slowly moving reference frame [Courtilot *et al.*, 2003]. Another model, based on numerical mantle flow modeling and seismic tomography, reproduces the observed latitudinal motion for the Hawaiian hot spot but predicts essentially no latitudinal motion for the Louisville hot spot [Steinberger *et al.*, 2004]. Even other models would abandon the mantle plume hypothesis altogether, explaining the Louisville seamount trail by (thermal) extension in the Pacific lithosphere or a genetic

relation with the Eltanin fracture zone [Smith and Lewis, 1999; Foulger and Natland, 2003].

[3] The paleolatitude data and $^{40}\text{Ar}/^{39}\text{Ar}$ age systematics of seamount trails provide us with the primary data to directly test these models. Where the paleolatitude data give us a location record of the volcanic source (or hot spot) over geological time and relative to the geocentric dipole, the age progressions are the sum of both plate and hot spot motions. It has been shown previously by Koppers *et al.* [2001] that $^{40}\text{Ar}/^{39}\text{Ar}$ age progressions along seamount trails are in most cases inconsistent with the fixed hot spot hypothesis, allowing for possible inter-hot spot motions up to 60 mm/yr. The differences in the observed age progressions thus are significant and allow us to distinguish between models of fixed and moving hot spots. It follows therefore that defining the $^{40}\text{Ar}/^{39}\text{Ar}$ age progressions along seamount trails accurately is critical to assessing hot spot and other models for intraplate volcanism (see review by Koppers *et al.* [2003b]).

[4] Watts *et al.* [1988] reported total fusion $^{40}\text{Ar}/^{39}\text{Ar}$ ages from nine seamounts that span the entire length of the Louisville seamount trail and that produced a surprisingly linear age progression (Figure 2). Since that time, $^{40}\text{Ar}/^{39}\text{Ar}$ techniques have been significantly improved by instrumental developments, better sample preparation methods, and more rigorous applications of the incremental

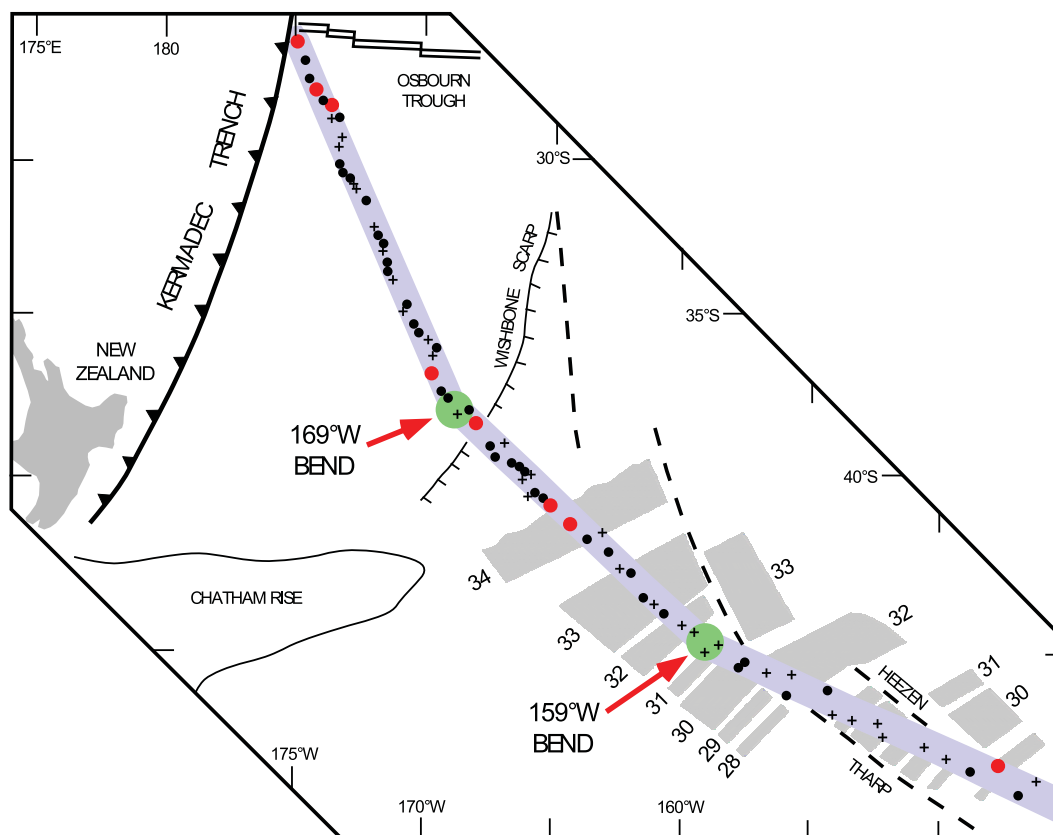


Figure 1. Location map of the Louisville seamount trail after *Lonsdale* [1988]. The seafloor magnetic anomalies [Cande and Kent, 1995], some important morphological features, and the fracture zones in the underlying oceanic basement are shown for reference. Two changes in orientation (bends) can be recognized in this seamount trail at 169°W and 159°W close to where it intersects with the Wishbone Scarp and Tharp fracture zone. Filled circles are guyots, and the plus signs indicate seamounts. Redated guyots are indicated by red circles. Note that the youngest dated sample, MTHN-7D1, falls off this map and is located at 50°26'S and 139°09'W.

heating technique. Submarine basalts can now be dated more accurately (and more precisely) because internal tests can be performed to identify samples that have been adversely affected by submarine alteration [Koppers *et al.*, 2000, 2003b]. This clearly makes the conventional K-Ar and total fusion $^{40}\text{Ar}/^{39}\text{Ar}$ techniques unsuitable for dating altered seamount basalts since both fall short in discriminating between fresh and altered seamount basalts and those affected by excess (mantle-derived) argon [cf. McDougall and Harrison, 1988].

[5] We have redated 10 samples from the *Watts et al.* [1988] study by applying high-resolution $^{40}\text{Ar}/^{39}\text{Ar}$ incremental heating experiments (Figure 3; Tables 1 and 2) that significantly improved the accuracy of the age determinations for the Louisville seamount trail. It is evident that samples older than 62 Ma have $^{40}\text{Ar}/^{39}\text{Ar}$ incremental heating ages that are older

than the previous ages determined by the total fusion technique (Table 3). A simple explanation is that these samples are too altered to provide reliable (total fusion) crystallization ages due to radiogenic ^{40}Ar and $^{39}\text{Ar}_k$ loss but that the incremental heating experiments were able to resolve these secondary processes and provide reliable age plateaus and isochrons.

[6] In this paper we present new high-resolution $^{40}\text{Ar}/^{39}\text{Ar}$ data for the Louisville seamount trail and discuss the systematics of groundmass dating for altered seamount basalts [cf. Koppers *et al.*, 2000]. Our new results show that the age progression for the Louisville seamount trail is not linear after all. We discuss the impact of the resulting nonlinear age progression on the important question of hot spot fixity and make comparisons with the new age systematics of the Hawaiian-Emperor seamount

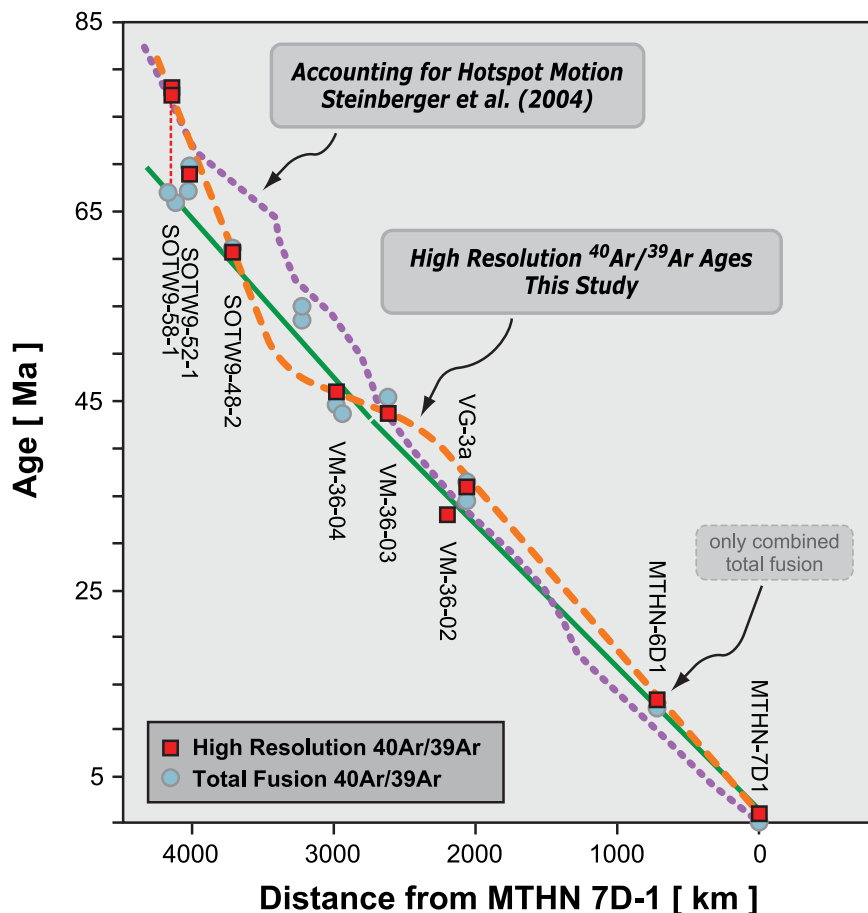


Figure 2. Comparison of new incremental heating ⁴⁰Ar/³⁹Ar ages with total fusion ages of *Watts et al.* [1988]. The new ages are up to 10–12 Myr older in the oldest part of the Louisville seamount trail (Table 3). Samples younger than 62 Myr are more compatible with previous total fusion ages, although the analytical precision in these age determinations is significantly improved (Table 3). The new incremental heating dates thus show a nonlinear age progression as indicated by the orange dashed line, which follows the oldest observed ages. An alternate age progression is shown by the purple dotted line as based on mantle convection models of *Steinberger et al.* [2004]. Their models allow for the movement of hot spots over geological time, which is reflected in a different age-distance relationship that is consistent with the older ages for Osborn seamount but not with the general age trend. More modeling results are shown in Figure 6.

trail [*Sharp and Clague, 2002; Tarduno et al., 2003*]. Finally, we present new results of mantle flow models that offer a possible explanation for the observed age systematics in both the Louisville and Hawaiian hot spot trails.

2. The ⁴⁰Ar/³⁹Ar Dating Techniques

[7] In total we performed 13 new ⁴⁰Ar/³⁹Ar incremental heating analyses on 10 samples from 9 seamounts or guyots in the Louisville seamount trail. This sample set contains 2 samples (SOTW-9-58-7 and VM36-02) that were not dated by *Watts et*

al. [1988]. The results of these incremental heating experiments are displayed in age plateau and isochron diagrams in Figure 3; the corresponding isotopic data are listed in Table 2. Analytical data can be downloaded from the EarthRef.org Digital Archive (ERDA) as detailed in Appendix A.

[8] The ⁴⁰Ar/³⁹Ar incremental heating age determinations were performed on crystalline ground-mass separates (250–500 μm) and one plagioclase mineral separate (250–500 μm) using a continuous, 10W CO₂ laser probe combined with a MAP-215/50 mass spectrometer at Oregon State Univer-

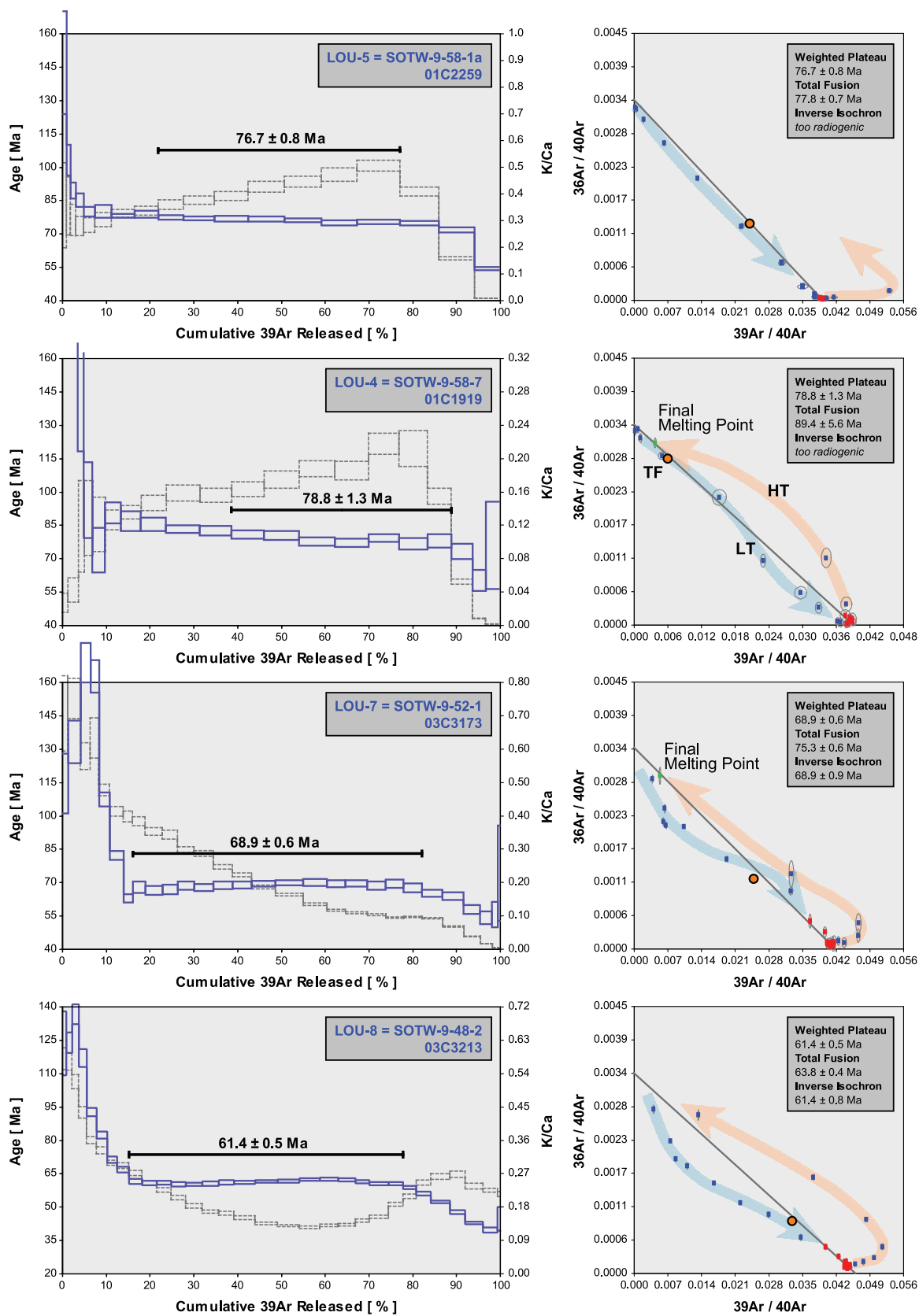


Figure 3

sity. Sample preparation and acid leaching are described by *Koppers et al.* [2000]. The mass spectrometer is a 90° sector instrument with a Nier-type source with an all-metal extraction system for $^{40}\text{Ar}/^{39}\text{Ar}$ age determinations. It has an electron multiplier for high sensitivity and an electrostatic analyzer with adjustable collector slit for an effective resolution (~ 600) of Ar peaks from small hydrocarbon peaks. Irradiated groundmass samples were loaded into Cu planchettes designed with a variety of pans that hold up to 50 mg of material, which are then pumped within a sample chamber fitted with a ZnSe window transparent to the CO_2 laser wavelength. Software allows for scanning across samples in a preset pattern with a defocused beam to evenly heat the material. Gas cleanup was accomplished with a series of Zr-Al getters. All argon ages were measured relative to the flux monitor standard FCT-3 biotite (28.04 ± 0.18 Ma, 1σ [*Renne et al.*, 1994]) and calculated using the corrected *Steiger and Jäger* [1977] decay constant of $5.530 \pm 0.097 \times 10^{-10}$ 1/yr (2σ) as reported by *Min et al.* [2000]. For a detailed description of the analytical facility and the constants used in the age calculations we refer to Table 2 of *Koppers et al.* [2003a]. Incremental heating plateau ages and isochron ages were calculated as weighted means with $1/\sigma^2$ as the weighting factor [*Taylor*, 1997] and as YORK2 least squares fits with correlated errors [*York*, 1969] using the ArArCALC v2.2 software from *Koppers* [2002], which is available from the <http://earthref.org/tools/ararcalc.htm> Web site. In this paper, all errors on the $^{40}\text{Ar}/^{39}\text{Ar}$ ages are reported at the 95% confidence level (2σ), unless otherwise indicated.

[9] To determine whether an incremental heating experiment yields meaningful crystallization ages, we adopted the following quality criteria proposed by *Fleck et al.* [1977] and *Pringle* [1993]: (1) high-temperature plateaus in the age

spectra should include more than three incremental heating steps and at least 50% of the total amount of $^{39}\text{Ar}_K$ released, (2) the plateau and isochron ages should be concordant at the 95% confidence level, (3) the $^{40}\text{Ar}/^{36}\text{Ar}$ intercepts on the isochron diagrams should be concordant with the atmospheric value of 295.5 at the 95% confidence level, and (4) the mean squared of weighted deviations (MSWD) [*York*, 1969; *Roddick*, 1978] for both the plateau ages (MSWD = SUMS/N-1) and isochron ages (MSWD = SUMS/N-2) should be sufficiently small when compared to Student's t test and F variance critical values for significance, respectively.

[10] Although these criteria are well suited for the evaluation of $^{40}\text{Ar}/^{39}\text{Ar}$ results from unaltered whole-rock samples and mineral separates, they are not necessarily suitable for the evaluation of altered basaltic groundmass separates [*Koppers et al.*, 2000]. There are several reasons for this. First of all, owing to the intensive acid leaching of the groundmass samples, the majority of the atmospheric component (from alteration, absorption, and trapped argon) is effectively removed from the samples, resulting in extremely high radiogenic components for the age plateaus. As a result, the dispersion in the data points is sometimes insufficient to calculate meaningful isochrons owing to a clustering of data points near the radiogenic intercept on the $^{39}\text{Ar}/^{40}\text{Ar}$ axis. Whenever the radiogenic components for all steps included in the age calculations are higher than 95%, we consider these data points too radiogenic to calculate meaningful isochrons (Figure 3). A second reason why groundmass analyses are harder to evaluate is the remaining alteration in the samples, even after intensive acid leaching. This remaining alteration typically causes MSWDs higher than 1, indicating an increased scatter due to geological uncertainties beyond the precision of the data points themselves.

Figure 3. High-resolution incremental heating $^{40}\text{Ar}/^{39}\text{Ar}$ analyses for Louisville seamount trail basalts. The reported $^{40}\text{Ar}/^{39}\text{Ar}$ ages are weighted age estimates with errors reported on the 95% confidence level, including 0.3–0.4% standard deviations in the J value. All samples were monitored against FCT-3 biotite (28.04 ± 0.18 Ma, 1σ) as calibrated by *Renne et al.* [1998]. Data are listed in Table 2, and ArArCALC age calculation files can be downloaded from the EarthRef.org Digital Archive (ERDA) as described in Appendix A. Note that “reference lines” are shown (defined by the 295.5 atmospheric intercept on the $^{36}\text{Ar}/^{40}\text{Ar}$ axis and by the plateau age on the $^{39}\text{Ar}/^{40}\text{Ar}$ axis) instead of the calculated isochrons.

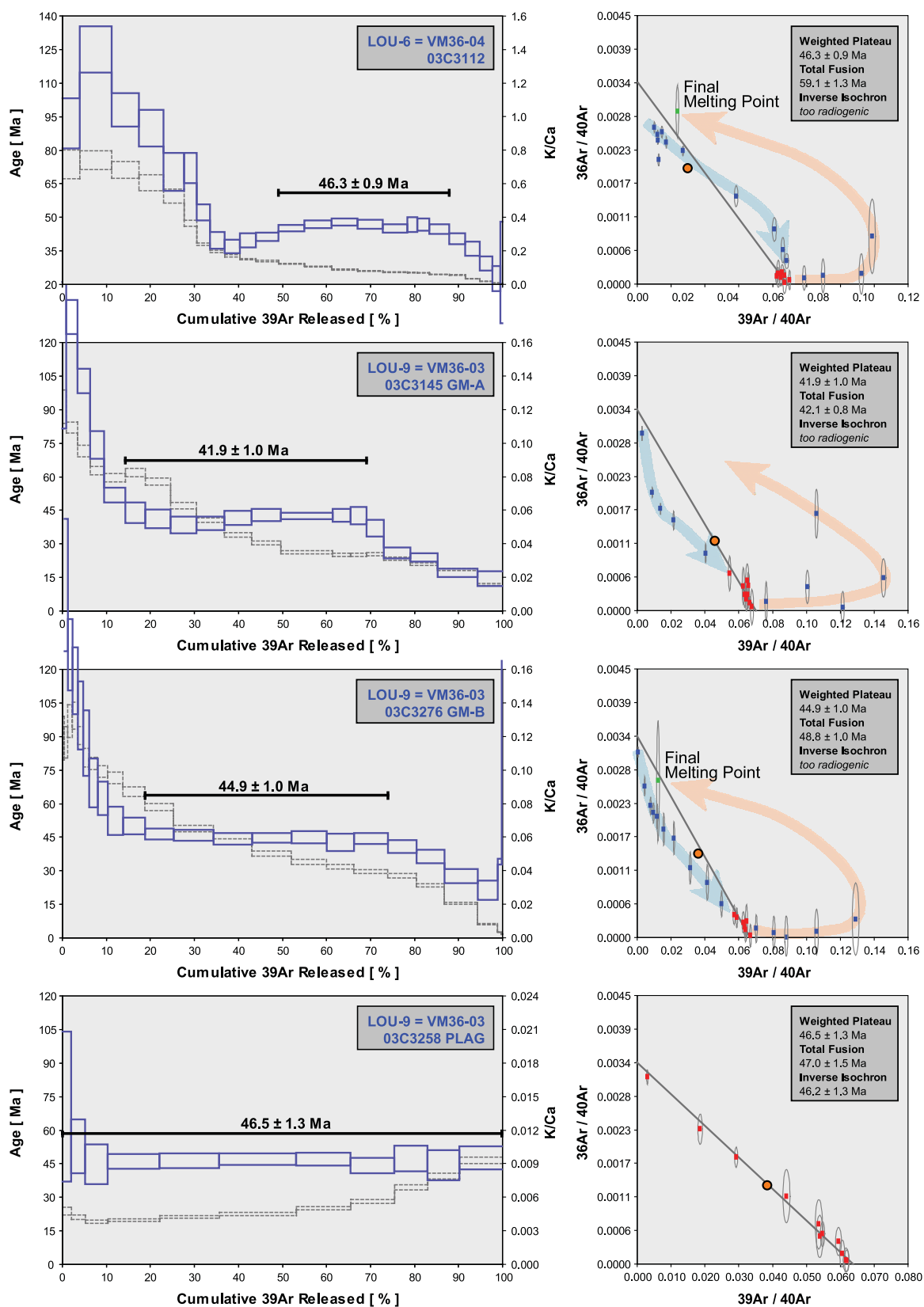


Figure 3. (continued)

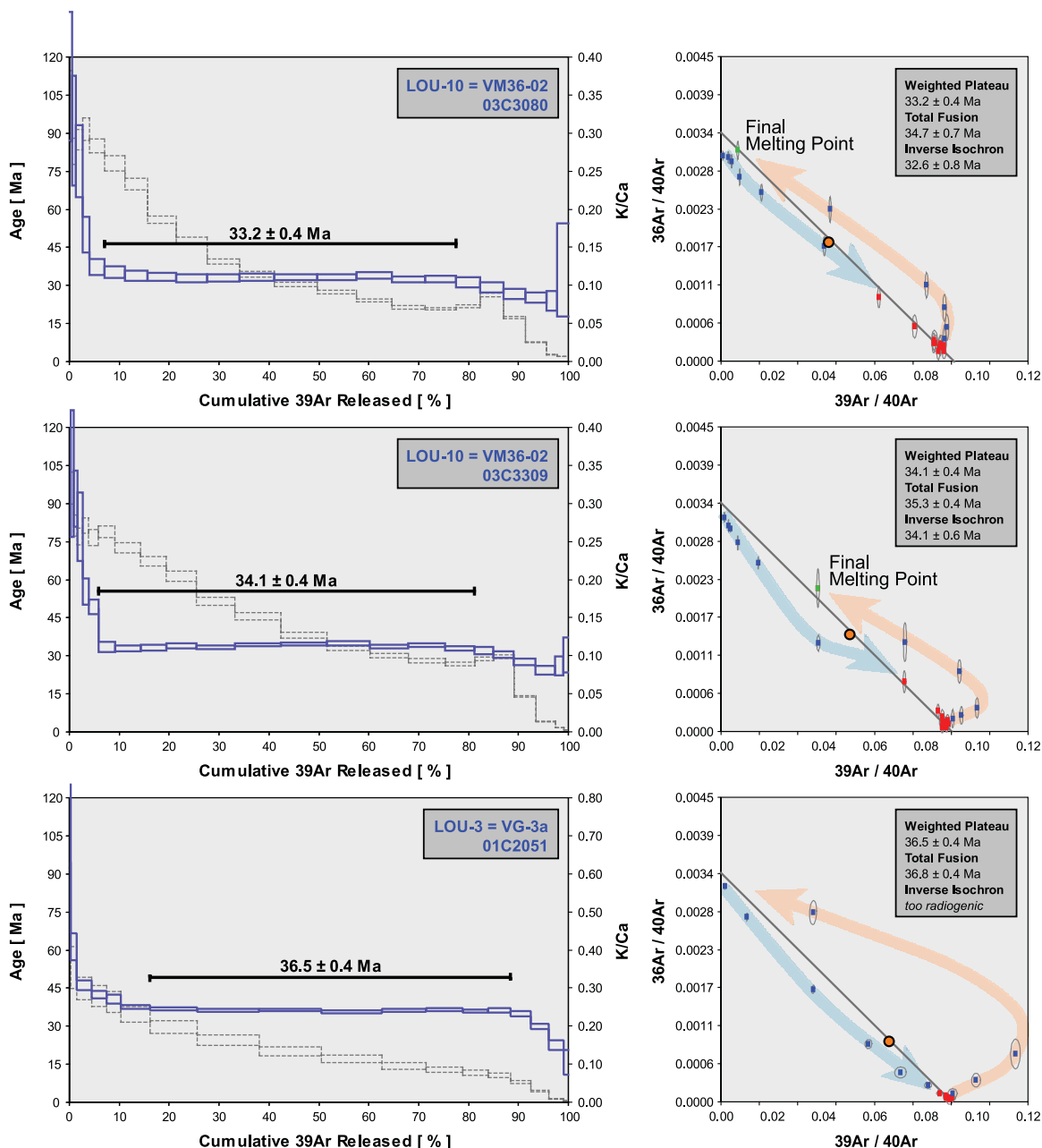


Figure 3. (continued)

In these cases the reported analytical errors are multiplied by the square root of MSWD [York, 1969; Kullerud, 1991]. The statistically maximum allowable MSWD is given by either the Student's t test for plateau ages or F variance test for isochron ages, which are both dependent on the number of data points included in the age calculations. If the MSWD is larger than this value, analytical errors alone cannot explain the scatter about the weighted

mean or isochron calculation, and ages derived from these calculations require further justification to be acceptable [Pringle, 1993].

3. Results and Discussion

[11] In this section we interpret the $^{40}\text{Ar}/^{39}\text{Ar}$ age spectra (Figures 3, 4, and 5) and assess the quality of the groundmass incremental heating experi-

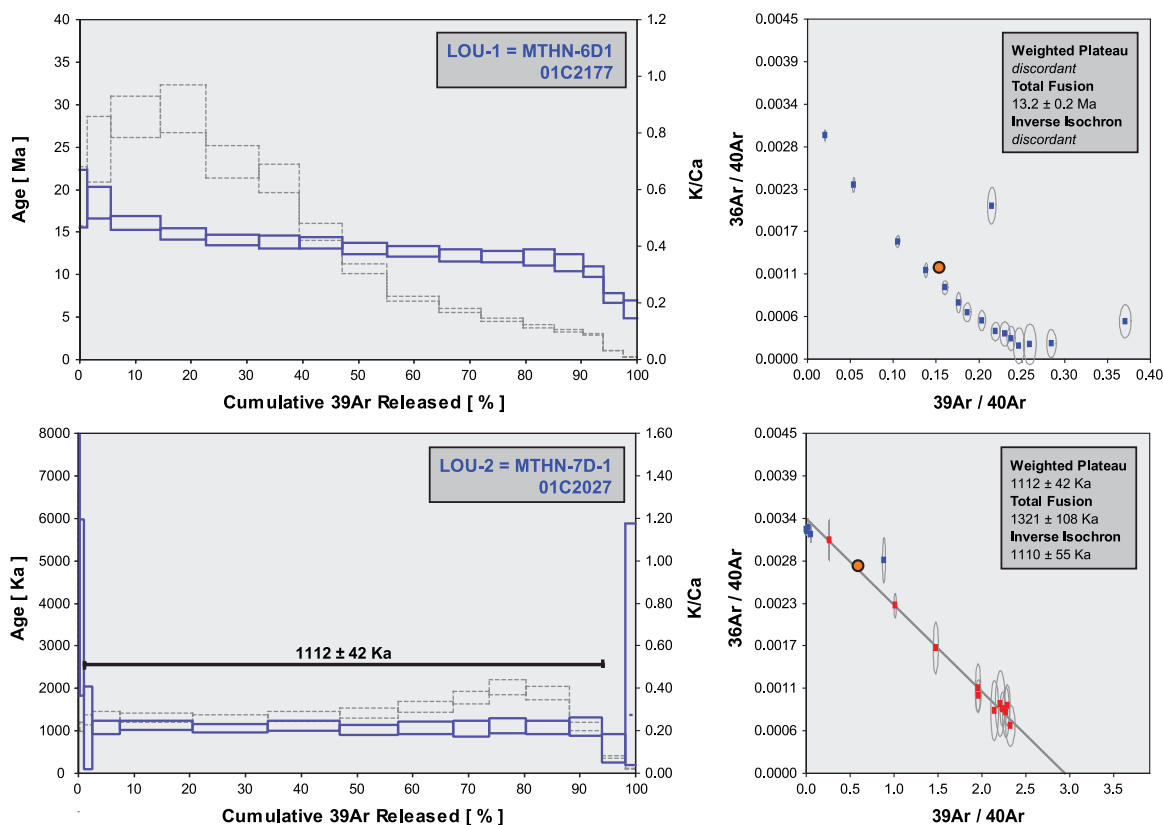


Figure 3. (continued)

ments. We discuss our new age results for the Louisville seamount trail in the context of various hot spot models, while addressing the nonlinear character of the observed age progression and its inferences for the motion of the Louisville hot spot. We finish by comparing the $^{40}\text{Ar}/^{39}\text{Ar}$ age progressions for the Louisville and Hawaiian-Emperor seamount trails and by using these data sets to calibrate and test new mantle flow models for the Pacific mantle.

3.1. The $^{40}\text{Ar}/^{39}\text{Ar}$ Geochronology of Seamount Basalts

[12] Although $^{40}\text{Ar}/^{39}\text{Ar}$ dating of seamount basalts by mineral separates (plagioclase, hornblende, biotite) in most cases is preferable over whole rocks due to their more homogenous degassing behavior, in reality we are limited by a lack of suitable phenocrystic materials in dredge collections. Out of necessity, dating basaltic groundmass samples using $^{40}\text{Ar}/^{39}\text{Ar}$ incremental heating techniques has become a powerful tool when studying

the evolution of seamount trails [Koppers *et al.*, 1998, 2003b]. It has been shown that crystalline groundmass samples can provide ages concordant with $^{40}\text{Ar}/^{39}\text{Ar}$ ages of comagmatic minerals and thus can be interpreted as eruption ages [Koppers *et al.*, 2000]. In this study we have applied the same groundmass dating technique to date the Louisville seamount basalts that are mildly alkalic with molar K/Ca ratios ranging from 0.05 to 0.38. Our high-resolution incremental heating experiments comprise 16–30 individual heating steps, allowing us to better resolve primary $^{40}\text{Ar}/^{39}\text{Ar}$ age signals from alteration and irradiation-induced disturbances. The resulting age spectra are normally well defined with wide age plateaus (32–75% of the total gas released) that include between 5 and 16 individual heating steps. The isotopic compositions for these age plateau steps generally show a reasonable dispersion in their radiogenic ^{40}Ar component (ranging between 80 and 100%) and result in isochrons with calculated $^{40}\text{Ar}/^{36}\text{Ar}$ intercept values indistinguishable from the atmospheric

Table 1. Sample Locations in the Louisville Seamount Trail

Sample Number	Seamount Name	Lat	Lon	Distance, km	Depth, mbsl	Rock Type	Cruise Name
<i>Northwestern Segment</i>							
SOTW-9-58-1a	Osbourm	25°31.8'S	174°02.4'W	4060	2443	basanite	SOUTHTOW09-1972
SOTW-9-58-7	Osbourm	25°31.8'S	174°02.4'W	4060	2443	olivine nephelenite	SOUTHTOW09-1972
SOTW-9-52-1		27°16.8'S	174°12.6'W	3919	3480	hawaiite	SOUTHTOW09-1972
SOTW-9-48-2	Currituck	30°06.0'S	173°15.0'W	3625	2300	hawaiite	SOUTHTOW09-1972
VM36-05		33°56.7'S	171°11.5'W	3175	2760	alkali basalt	VEMA36-02-1979
<i>Middle Segment</i>							
VM36-04		36°57.0'S	169°50.0'W	2856	1446	picritic basalt	VEMA36-02-1979
VM36-03		38°19.5'S	167°43.7'W	2616	1232	alkali basalt	VEMA36-02-1979
VM36-02		40°47.0'S	165°21.0'W	2286	1883	alkali basalt	VEMA36-01-1979
VG-3a/MSN110-1	Valerie	41°36.8'S	164°12.0'W	2154	950	alkali basalt	MONSOON07-1961
<i>Southeastern Segment</i>							
MTHN-6D1		48°12.0'S	148°48.0'W	742	720	alkali basalt	MARATHON06-1984
MTHN-7D1		50°26.0'S	139°09.0'W	0	640	alkali basalt	MARATHON06-1984

ratio, ruling out excess ^{40}Ar . It is noteworthy that most of the “final melting points” (not included in the isochron calculations) project toward the “reference line” between the atmospheric intercept on the $^{36}\text{Ar}/^{40}\text{Ar}$ axis and the argon age intercept on the $^{39}\text{Ar}/^{40}\text{Ar}$ axis (Figure 3). This indicates that the trapped argon in the groundmass samples has an initial $^{40}\text{Ar}/^{36}\text{Ar}$ ratio close to the 295.5 value in modern air. Finally, the total fusion points also fall close to or on these reference lines (see the orange circles in Figure 3), indicating that the isochron, plateau, and total fusion ages are usually concordant at the 2σ confidence level and that most discordances observed in our age plateaus are due to recoil redistribution of reactor-produced argon isotopes. These observations are all good indicators of the good quality of the $^{40}\text{Ar}/^{39}\text{Ar}$ groundmass ages on these seamount basalt samples.

[13] The groundmass argon release patterns thus prove to be characteristic (Figures 3 and 4) and allow us to explain the degassing behavior of (holo)crystalline groundmass samples during incremental heating experiments (Figure 5). The low-temperature (LT) increments are typically characterized by high apparent ages, high K/Ca ratios, and significant spikes in the $^{36}\text{Ar}_{\text{atm}}$ and $^{38}\text{Ar}_{\text{cl}}$ components that reflect high contributions in the total argon inventory from atmospheric com-

ponents and chlorine. All of these observations can be explained by the recoil of $^{39}\text{Ar}_{\text{K}}$ (high apparent ages) as associated with the preferential degassing of fine-grained alteration phases (high K/Ca ratios; high atmospheric and chlorine contents) that remain in the groundmasses, even though the samples were treated by intensive acid leaching [Koppers *et al.*, 2000]. Electron microprobe analyses have shown that this remaining alteration is most likely located interstitially and on the surfaces of groundmass minerals [Koppers *et al.*, 2000]. In the isochron diagrams the discordant LT steps start off from the atmospheric intercept on the $^{36}\text{Ar}/^{40}\text{Ar}$ axis, followed by a curved approach toward the isochron, as shown by the light blue arrows in Figure 3. These concave curves are best explained by the degassing of predominantly alteration phases at the lowest temperatures (light blue circles) and an increasing contribution of primary groundmass degassing (pink circles) with higher temperatures, generating subhorizontal mixing lines in the isochron diagrams (Figure 5). During degassing the atmospheric component continuously diminishes until the released argon gasses for individual heating steps are about 80–100% radiogenic (Figure 4). This latter process causes a decreasing $^{36}\text{Ar}/^{40}\text{Ar}$ trend in isochron diagrams. In reality, all three processes start to act together almost immediately following the onset of the

Table 2. Incremental Heating $^{40}\text{Ar}/^{39}\text{Ar}$ Analyses on Louisville Seamount Basalts^a

Sample Number	Lab Code	Experiment Number	Sample Type	Age Spectrum				Total Fusion		Inverse Isochron Analyses		
				Age $\pm 2\sigma$, Ma	^{39}Ar , %	K/Ca	MSWD	n	Age $\pm 2\sigma$, Ma	Age $\pm 2\sigma$, Ma	$^{40}\text{Ar}/^{36}\text{Ar}$ Intercept	MSWD
<i>Northwestern Segment</i>												
SOTW-9-58-1a	LOU-5	01C2259	groundmass	76.7 \pm 0.8	55	0.415	2.8	7	77.8 \pm 0.7			
SOTW-9-58-7	LOU-4	01C1919	groundmass	78.8 \pm 1.3	50	0.179	2.4	7	89.4 \pm 5.6			
SOTW-9-52-1	LOU-7	03C3173	groundmass	68.9 \pm 0.6	67	0.132	1.5	15	75.3 \pm 0.6	68.9 \pm 0.9	294.8 \pm 110	1.7
SOTW-9-48-2	LOU-8	03C3213	groundmass	61.4 \pm 0.5	63	0.154	3.8	16	63.8 \pm 0.4	61.4 \pm 0.8	298.9 \pm 81.7	4.1
<i>Middle Segment</i>												
VM36-04	LOU-6	03C3112	groundmass	46.3 \pm 0.9	39	0.072	1.6	8	59.1 \pm 1.3			
VM36-03	LOU-9	03C3145	groundmass A	42.5 \pm 1.1	32	0.036	0.1	5	42.1 \pm 0.8			
		03C3276	groundmass B	44.9 \pm 1.0	55	0.050	0.7	7	48.8 \pm 1.0			
		03C3258	plagioclase C	46.5 \pm 1.3	100	0.005	0.6	11	47.0 \pm 1.5	46.2 \pm 1.3	304.5 \pm 10.8	0.4
VM36-02	LOU-10		combined A + B + C	44.5 \pm 0.8			1.6	23	45.5 \pm 0.6	44.3 \pm 0.8	310.1 \pm 12.6	1.3
			combined B + C	45.5 \pm 0.8			0.8	18	47.8 \pm 0.9	45.3 \pm 0.8	306.6 \pm 10.8	0.6
			groundmass A	34.1 \pm 0.4	75	0.123	2.8	11	35.3 \pm 0.4	34.1 \pm 0.6	294.0 \pm 129	3.1
VG-3a/MSN110-1	LOU-3	03C3309	groundmass B	33.2 \pm 0.4	70	0.094	0.9	11	34.7 \pm 0.7	32.6 \pm 0.8	357.1 \pm 68.8	0.5
		03C3080	combined A + B	33.9 \pm 0.3	73	0.105	2.4	22	35.0 \pm 0.4	33.8 \pm 0.5	314.0 \pm 68.9	2.5
		01C2051	groundmass	36.5 \pm 0.4	72	0.094	1.5	8	36.8 \pm 0.4			
<i>Southeastern Segment</i>												
MTHN-6D1	LOU-1	01C2177	groundmass						13.2 \pm 0.2			
MTHN-7D1	LOU-2	01C2027	groundmass	1.112 \pm 0.042	93	0.275	0.3	11	1.321 \pm 0.108	1.110 \pm 0.055	296.9 \pm 18.7	0.4

^a K/Ca values are calculated as weighted means for the age spectra or using recombined totals of $^{39}\text{Ar}_g$ and $^{37}\text{Ar}_{Ca}$ for the total fusions. MSWD values for the age plateaus and inverse isochrons are calculated using N-1 and N-2 degrees of freedom, respectively. All samples from this study were monitored against FCT-3 biotite (28.04 \pm 0.18 Ma) as calibrated by Renne *et al.* [1998]. Reported errors on the $^{40}\text{Ar}/^{39}\text{Ar}$ ages are on the 95% confidence level, including 0.3–0.4% standard deviation in the J value. All input parameters to the calculations are published in Table 2 of Koppers *et al.* [2003a]. Note that two groundmass samples for VM36-03 have been listed, which represent two different selections of groundmass grains based on their colorizations. Grains in Groundmass A are more “whitish,” indicating zeolite alteration, whereas grains in Groundmass B are more “dark grayish,” indicating fresher grains. It is likely that the lower age of Groundmass A is a direct result of increased seawater alteration.

Table 3. Comparison of ⁴⁰Ar/³⁹Ar Total Fusion and High-Resolution Incremental Heating Ages^a

Sample Number	Lab Code	This Study (2003)		<i>Watts et al.</i> [1988]		Differences	
		Age ± 2σ, Ma	n	Age ± 2σ, Ma	Repeat, Ma	Age, %	Error, %
<i>Northwestern Segment</i>							
SOTW-9-58-1a	LOU-5	76.7 ± 0.8	1	67.2 ± 1.2	66.5 ± 1.2	15%	−33%
SOTW-9-58-7	LOU-4	78.8 ± 1.3	1				
SOTW-9-52-1	LOU-7	68.9 ± 0.6	1	67.3 ± 2.8	70.7 ± 2.8	0%	−79%
SOTW-9-48-2	LOU-8	61.4 ± 0.5	1	61.7 ± 1.8		0%	−72%
VM36-05				53.9 ± 5.2			
<i>Middle Segment</i>							
VM36-04	LOU-6	46.3 ± 0.9	1	45.0 ± 1.0		3%	−10%
VM36-03	LOU-9	45.5 ± 0.8	2	45.9 ± 1.0		−1%	−20%
VM36-02	LOU-10	33.9 ± 0.3	2				
VG-3a/MSN110-1	LOU-3	36.5 ± 0.4	1	36.9 ± 1.2	34.7 ± 1.2	−1%	−67%
<i>Southeastern Segment</i>							
MTHN-6D1	LOU-1	13.2 ± 0.2	1	12.6 ± 0.8		5%	−75%
MTHN-7D1	LOU-2	1.112 ± 0.042	1	0.5 ± 0.4		122%	−89%

^aThe difference in age is most prominent for Osborn seamont with a 15% increase, whereas the youngest sample dated has been more than doubled in age when compared to the total fusion age. The precision has increased for all samples by showing 10–89% improvements. Note that *Watts et al.* [1988] used MMhb-1 calibrated by *Dalrymple et al.* [1981] at 519.5 ± 2.5 Ma (1σ) to calibrate its internal ⁴⁰Ar/³⁹Ar ages, whereas this study uses FCT-3 at 28.04 ± 0.18 Ma [*Renne et al.*, 1998]. To make age comparisons possible, we used the ArArCALIBRATIONS tool (Appendix A) to recalibrate the *Watts et al.* [1988] ages toward the FCT-3 standard based on the explicit age equations of *Min et al.* [2000] as detailed by *Koppers* [2002].

incremental heating, resulting in a more “curved” array of data points, as is usually observed in the isochron diagrams (Figure 3).

[14] Well-resolved age plateaus develop at the intermediate temperature steps that are high in their radiogenic ⁴⁰Ar component and that show almost no contribution from the ³⁸Ar_{c1} component (Figure 4). We conclude therefore that the effects of alteration and ³⁹Ar_K recoil are almost negligible in the age plateaus. However, some of these age plateaus may still reveal subtle systematic changes, such as declining or arching upward age profiles, that can be attributed to the lingering effects of alteration and recoil on the age spectra. Groundmass experiments SOTW-9-58-1a and SOTW-9-48-2 are good examples showing these subtle changes. In the case of SOTW-9-58-1a we observe a monotonically declining age plateau with a slope of −0.069 Ma/% that results in an age difference of 4.9 Ma between the beginning (5%) and end (77%) of the widest possible age plateau. This sloping exceeds the 95% confidence envelop and thus does not constitute an age plateau *senso stricto*. As a result, the calculated plateau age of 77.2 ± 0.9 Ma (*n* = 11) is associated with a high

MSWD of 5.3, indicating scatter beyond analytical error. Instead, we prefer to define an age plateau from higher release temperatures, resulting in an age of 76.7 ± 0.8 Ma with a lower MSWD of 2.8 (Table 2) that is only slightly higher than the allowable Student’s *t* value of 2.5 for *n* = 7. We argue that this plateau is a better estimate for the eruption age of this sample since the effects of alteration and recoil would have been further diminished owing to the extra heating of the groundmass sample (Figure 5), even though the total fusion age of 77.8 ± 0.7 Ma is concordant with both plateau age estimates. In the case of SOTW-9-48-2 we have an arching upward age spectrum with a MSWD of 3.8 that is above the allowable Student’s *t* value of 2.1 for *n* = 16. Despite the slightly large MSWD, we still believe that this age of 61.4 ± 0.5 Ma represents the best estimate of the eruption age since the plateau and isochron ages are concordant on the 2σ level and the total fusion age is very close as well at 63.8 ± 0.8 Ma.

[15] The interpretation of two groundmass analyses and one plagioclase analysis for alkali basalt VM36-03 is not unequivocal either, where the plagioclase age of 46.5 ± 1.3 Ma is discordant

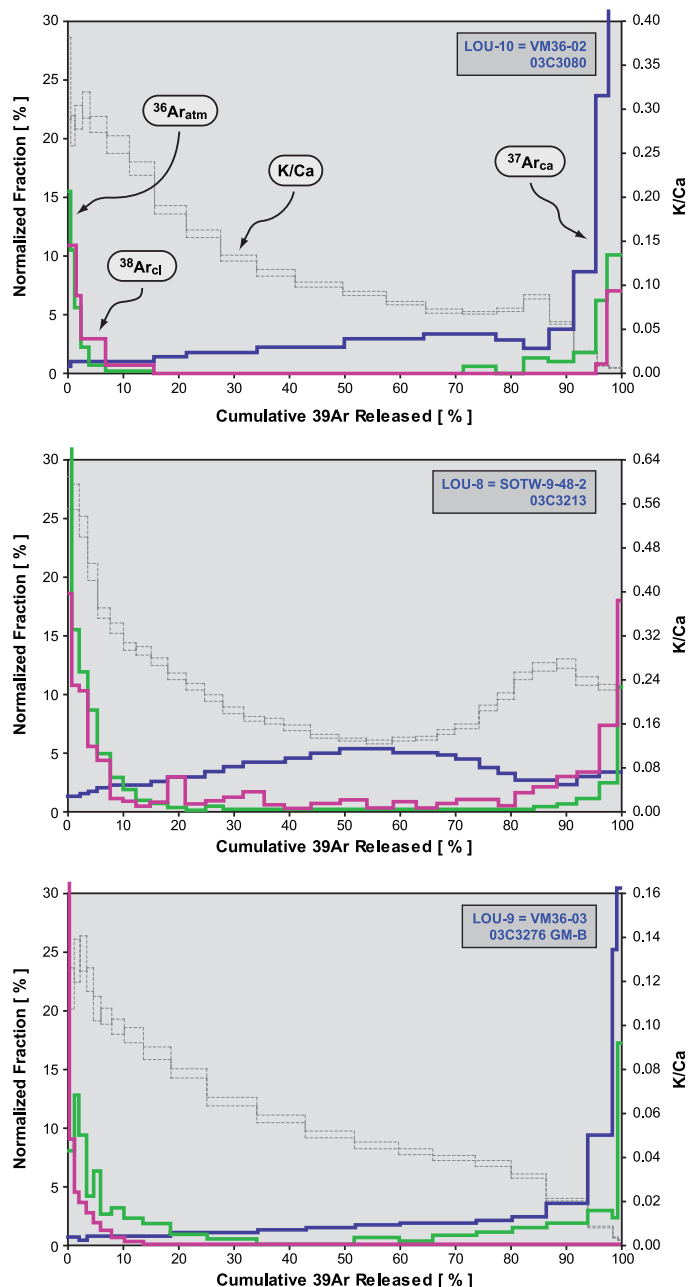


Figure 4. Examples of typical degassing behavior in the groundmass $^{40}\text{Ar}/^{39}\text{Ar}$ analyses. In this representation we display for each increment the fraction of the $^{36}\text{Ar}_{\text{atm}}$ and $^{37}\text{Ar}_{\text{ca}}$ and $^{38}\text{Ar}_{\text{cl}}$ components relative to the total amount of gas released during the experiment. These percentages have been normalized to the size of each degassing step, as approximated by the size of the $^{39}\text{Ar}_k$ component. Clear changes in gas composition (i.e., spikes) are visible at the beginning and the end of each degassing spectra, reflecting the degassing of alteration products at low temperatures and high-Ca minerals, such as plagioclase and clinopyroxene, at high temperatures.

with groundmass A (42.5 ± 1.1 Ma) but is concordant with groundmass B (44.9 ± 1.0 Ma). The question here is, what determines the difference in the groundmass ages? Both groundmasses have undergone the same sample treatment, except that

we selectively handpicked different colored grains from the groundmass separate. Groundmass A contained the more “whitish” grains, a coloration that is indicative of zeolite alteration, whereas groundmass B contained the more “dark grayish”

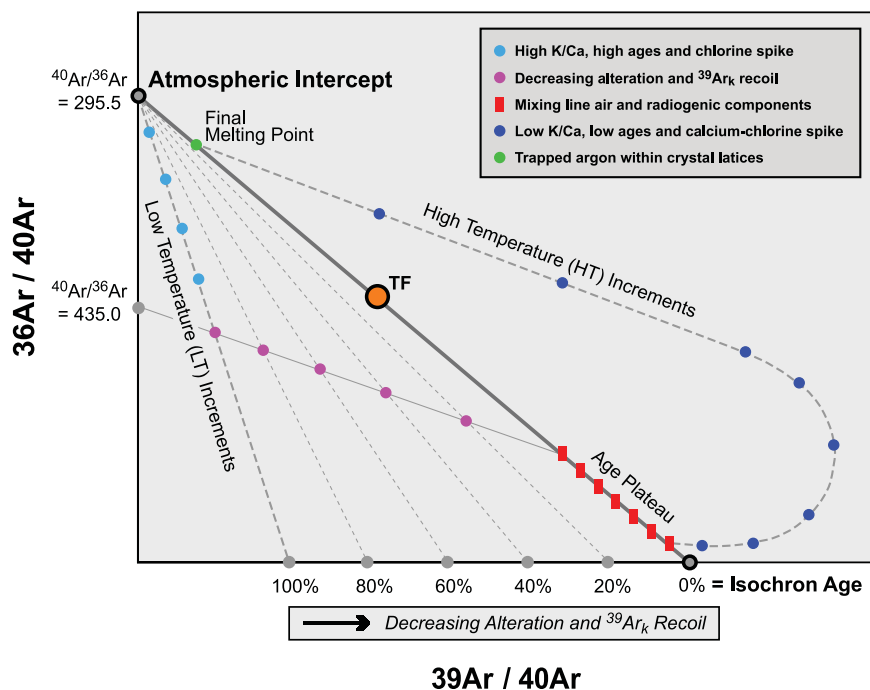


Figure 5. Schematic isochron diagram explaining the low- and high-temperature deviations routinely observed in groundmass $^{40}\text{Ar}/^{39}\text{Ar}$ analyses as caused by submarine alteration. This diagram shows that disturbances due to alteration can be resolved by performing high-resolution incremental heating experiments (15–30 increments) on groundmasses that have been cleaned with an enhanced acid-leaching procedure. After Koppers *et al.* [2000].

colored grains that normally represent the fresher groundmass. The results of this can be seen in the age spectrum of groundmass A, which does not have a simple horizontal and wide age plateau as groundmass B does. Instead, the age plateau is arching up significantly, where the top of the bulge gives the best approximation to the eruption age of this sample, which seems markedly lower than the age estimates from groundmass B and the plagioclase. However, when combining all age plateau steps from groundmasses A and B and the plagioclase, we calculate a new weighted mean age of 44.5 ± 0.8 Ma with a MSWD of 1.6 for $n = 23$ (Table 2). This MSWD is well within the range of the allowable Student's t value of 2.1 for this number of data points. Thus the individual ages for the incremental heating steps in the age plateau for groundmass A are concordant within the total population of measurements on sample VM36-03. In fact, if one were to plot the age plateaus on top of each other, one would see that these individual age boxes are (just barely) overlapping with the age boxes of groundmass B and the plagioclase at

the 2σ confidence level. Having said all of this, it is clear that the data are not easy to interpret since alteration plays a more important role in groundmass A than in groundmass B. Since the plagioclase age is certainly concordant with groundmass B, we use the combined age of groundmass B and the plagioclase analyses of 45.5 ± 0.8 Ma (Table 2) in our modeling.

[16] In most cases the plateau ages thus approximate the eruption ages, as is confirmed by the facts that most plateau ages are consistent with the corresponding isochron and total fusion ages and that the $^{40}\text{Ar}/^{36}\text{Ar}$ intercept values are indistinguishable from the 295.5 atmospheric ratio. It is important to note here that in the inverse isochron diagrams the data points representing the age plateaus form clear arrays (red squares) running parallel to the “reference line” between the plateau age on the $^{39}\text{Ar}/^{40}\text{Ar}$ axis and the 295.5 atmospheric intercept on the $^{36}\text{Ar}/^{40}\text{Ar}$ axis (Figures 3 and 5). These arrays form distinct linear segments with different angles compared to the discordant low-

and high-temperature data points, which indicates that the age plateaus are not (significantly) affected by the same secondary (alteration) processes and disturbances. Instead, they represent bimodal mixing lines between the radiogenic and atmospheric components.

[17] Relative to the plateau-forming increments, the high-temperature (HT) steps are characterized by minor (but significant) decreases in their apparent age, strong decreases in the K/Ca ratios, and large increases in the $^{37}\text{Ar}_{\text{Ca}}$ and $^{36}\text{Ar}_{\text{atm}}$ components (Figure 4) that reflect the preferential degassing of clinopyroxene and plagioclase minerals. In some cases a second increase is observed for the $^{38}\text{Ar}_{\text{Cl}}$ component (Figure 4) that might be related to the primary chlorine contents of clinopyroxene and plagioclase in the crystalline groundmass samples. These changes in argon composition coincide with the onset of melt glazing during the incremental heating experiments, indicating that congruent partial melting of the groundmass mineral assemblage has started. These discordant HT steps show a clear departure from the isochrons, as is indicated by the light orange arrows in Figure 3. These convex curves first move toward higher $^{39}\text{Ar}/^{40}\text{Ar}$ ratios and then quickly toward the atmospheric intercept for the final heating steps, where they sometimes intersect with the reference line (see dark blue circles in Figure 5). These so-called “final melting points” (FMPs) form a new observation that supports the assumption that trapped argon has a value for $^{40}\text{Ar}/^{36}\text{Ar}$ close to 295.5 for these groundmass samples (compare the green symbols in Figure 3). It is an independent observation since the FMPs are not included in the isochron calculations. They represent the last step in an incremental heating experiment that should entirely melt the groundmass sample (at the highest possible temperatures), releasing the final portion of argon gas. It is our reasoning that these last portions represent the trapped argon between crystal lattices. Yet, as can be seen in some of the isochron diagrams, not all FMPs fall on the “reference line” or close to it. This is not entirely unexpected for two reasons. First, by using a CO_2 laser it is difficult to reach these high temperatures in order to totally degas the samples. Second, in a two-component mixing sys-

tem it is very uncommon to sample the end-members themselves. Our argument thus is that the FMPs project toward the intercept of the reference line on the $^{36}\text{Ar}/^{40}\text{Ar}$ axis, close to atmospheric argon. It is noteworthy that the FMPs never fall under the reference line, which would be a definite sign of the presence of excess argon.

[18] We have shown that dating crystalline groundmass samples provides $^{40}\text{Ar}/^{39}\text{Ar}$ ages that are reliable estimates of the eruption ages of seamount basalts, in particular, in absence of suitable potassium-bearing minerals to be dated. These improved ages paint a different picture in terms of the age progression along the Louisville seamount trail, when compared to the original *Watts et al.* [1988] study, and have important consequences for the fixed hot spot model.

3.2. Analyses of the Nonlinear Age Progression

[19] We have redated most samples from the *Watts et al.* [1988] except those that were judged too glassy or too altered. We were able to add two new age determinations for samples SOTW-9-58-7 and VM36-02, which were dredged from Osborn Seamount in the northwestern segment and an unnamed seamount in the middle segment of the Louisville seamount trail (Figure 1). On the basis of improved methodology we significantly increased both the accuracy and precision (10–89% improvements) when compared to the total fusion ages of the *Watts et al.* [1988] study (Table 3). The new ages are 10–12 Myr (15%) older in the oldest part of the Louisville seamount trail. This clearly indicates a significant change in “apparent” plate versus hot spot velocity for the Pacific plate prior to 62 Ma when compared to previous studies on Pacific plate motion [e.g., *Duncan and Clague*, 1985; *Lonsdale*, 1988; *Wessel and Kroenke*, 1997; *Koppers et al.*, 2001]. Samples younger than 62 Myr are more compatible with the previous total fusion ages, confirming the linear trend between 47 Ma and the present day (although based on only three samples over 2150 km). We were also able to date the most recent volcanic activity at the Louisville seamount trail at 1.11 ± 0.04 Ma for the most southeastern seamount at $50^\circ 26' \text{S}$, $139^\circ 09' \text{W}$.

[20] The new incremental heating ages thus show a nonlinear age progression, indicated by the orange dashed line in Figure 2, that follows the oldest observed ages along the Louisville seamount trail. This preferred age progression includes only the high-resolution incremental heating ages from this study; it unfortunately does not include a reanalysis of the ~ 55 Ma total fusion age for sample VM-36-05 [Watts *et al.*, 1988] since it contains too much volcanic glass to be useful for $^{40}\text{Ar}/^{39}\text{Ar}$ dating. Nonetheless, the new age database includes some important new analytical constraints that support the validity of this nonlinear age progression. The upward bulge near 45 Ma is tightly constrained by the VG-3a groundmass of 36.5 ± 0.4 Ma and the VM36-03 plagioclase of 46.5 ± 1.3 Ma. Both ages conform to the quality criteria outlined in this paper, with 72% and 100% of the total amount of argon gas included in the age plateaus for 8 and 11 incremental heating steps and with internally concordant plateau, total fusion, and isochron ages at the 95% confidence level. The older age for Osborn guyot is most remarkable and is confirmed by two age determinations (76.6 ± 0.8 Ma; 78.8 ± 1.3 Ma) on two separate rocks, even though they might indicate some significant duration of volcanism at Osborn.

[21] An alternate age progression is shown by the purple dotted line, as based on mantle convection models of Steinberger *et al.* [2004]. Their models allow for the movement of the Louisville hot spot over geological time, which is reflected in a different age-distance relationship that is consistent with the older ages for Osborn seamount but not with the general age trend at the older end of the seamount trail. Adjusted models show a better agreement, as discussed in the next paragraph.

3.3. Evaluating Mantle Flow Models Allowing for Hot Spot Motion

[22] We now evaluate whether the motion of hot spots derived from current models of mantle flow, in combination with plate rotation models, are adequate to explain the geometries and age progressions of the Hawaiian and Louisville seamount trails, and for which model parameters we find the best fit to the highest-quality age data, including

the new $^{40}\text{Ar}/^{39}\text{Ar}$ ages reported in this paper. These models have been previously described in more detail [e.g., Steinberger and O'Connell, 1998; Steinberger, 2000] and include two steps. In the first step, a large-scale mantle flow field is computed on the basis of internal density heterogeneities as inferred from seismic tomography studies, the viscosity structure of the mantle, and plate motions. In the second step a plume conduit is inserted into this flow field, which rises vertically in the beginning but subsequently is advected into the large-scale mantle flow while rising buoyantly. The source of this conduit is assumed to move with the horizontal flow component in the lowermost mantle. In this discussion we will use the same modeling assumptions as in the "moving source models" of Steinberger *et al.* [2004] and Tarduno *et al.* [2003] except where specifically noted. We will begin this discussion by considering the Hawaiian and Louisville hot spots as part of the Pacific convection system only, but we will conclude with models that try to optimize the fit to all global hot spot tracks and the global plate motion circuit, in an approach similar to Steinberger *et al.* [2004]. All tracks shown are computed for Pacific plate motion with no boundary or intraplate deformation between the north and south Pacific.

[23] For comparison reasons, we start out by showing the best fitting tracks and age progressions for fixed hot spots (case 0, black lines) as modeled for the Pacific plate motion only. Four stages of constant Pacific plate rotation are allowed, with a major plate motion change at 47 Ma that marks the revised age of the bend in the Hawaiian-Emperor seamount trail [Sharp and Clague, 2002]. Another change in plate motion around 62 Ma permits an improved fit to the age progression of the older part of the Louisville seamount trail, as new high-resolution $^{40}\text{Ar}/^{39}\text{Ar}$ ages indicate a slower plate motion prior to 62 Ma. In this fixed hot spot case the computed ages for the older part of the Hawaiian track tend to be too old by ~ 10 Ma, while its geometry is poorly fitted. Also, the computed ages for the older part of the Louisville seamount trail are too young by ~ 5 Ma. These results may seem surprising at first, since the combination of both the Hawaiian and Louisville

hot spot tracks was used previously to support the fixed hot spot hypothesis [e.g., *Morgan*, 1972; *Duncan and Richards*, 1991]. However, this conclusion can be readily understood by considering how radiometric age dates have changed recently for the Hawaiian-Emperor and Louisville seamount trails. Ages for Detroit Seamount at the northern end of the Emperor seamount trail reported by *Tarduno et al.* [2003] are younger than previously determined [*Keller et al.*, 1995], whereas the Hawaiian-Emperor bend now appears to be about 4 Myr older than previously assumed, at 47 Ma [*Sharp and Clague*, 2002]. As a consequence, the motion of the Pacific plate relative to the Hawaiian hot spot during the formation of the Emperor chain now appears significantly faster than previously understood. In contrast, on the basis of the $^{40}\text{Ar}/^{39}\text{Ar}$ age dates reported in this paper, the motion of the Pacific plate relative to the Louisville hot spot during the same time interval now appears slower (Figure 2). While previous results supported the idea that the Hawaiian and Louisville hot spots are fixed relative to each other, the new results are better explained with a closing motion between the hot spots, particularly prior to 62 Ma. On the basis of the results from this study, we expect that the difference between the ancient paleolatitudes of the Louisville seamount trail and the present-day latitude of its hot spot is not as large as the difference between paleolatitudes of the Emperor seamount trail and the current location of the Hawaiian hot spot. We anticipate that it will be possible to confirm or refute this model prediction through future ocean drilling.

[24] The dashed orange lines in Figure 6 show the best fitting tracks (left panels) and age progressions (right panels) for a model of Hawaiian and Louisville hot spot motion (case 1) modified after *Steinberger et al.* [2004]. Recent geochemical and paleomagnetic results [*Mahoney et al.*, 1993; *Tejada et al.*, 1996; *Neal et al.*, 1997; *Antretter et al.*, 2004] make it appear less likely that the Louisville hot spot and Ontong Java Plateau are genetically linked, allowing us to use a plume initiation age of 90 Ma that is much younger than the ~ 122 Ma age of the Ontong Java Plateau. A southeastward motion is

computed for the Louisville hot spot. This modified model yields a very good overall fit to the geometry and age progression of the Hawaiian and Louisville seamount trails. In particular, the $^{40}\text{Ar}/^{39}\text{Ar}$ ages of the older parts of the Louisville and Hawaiian seamount trails fit increasingly well. This does not contradict the finding that the new age determinations indicate a slower plate motion relative to the Louisville hot spot in the 80–62 Ma period, as we can achieve a good fit for that period by choosing a slower plate motion. Obviously, it may also be caused by a slower hot spot motion during that period; however, this does not occur in our numerical models. Using a younger plume initiation age is one way to achieve a better fit in these models, but there may be other ways as well. Owing to the considerable spread of model results, the fact that an initiation age of 90 Ma yields a better fit than 120 Ma does not comprise new evidence for disconnecting the formation of the Ontong Java Plateau from the Louisville hot spot.

[25] The Louisville hot spot motion computed under different modeling assumptions may thus vary considerably. The average of a large number of model runs is a slow eastward to southeastward motion over the last 90 Myr. In contrast to Hawaii, where the modeled hot spot motion essentially represents the straightening up of a conduit that had been strongly tilted prior to 80 Ma, the Louisville hot spot motion approximately represents horizontal flow in the upper part of the lower mantle away from the subduction zones that are located to the west of the Louisville seamount trail (Figure 1). Contributions to this pattern are (1) a deep return flow opposite to Pacific plate motion, (2) a flow outward from the upwelling “superplume” beneath the South Pacific that is toward the south in the vicinity of Louisville, and (3) for some models, including the one used here, flow outward from a regional upwelling southeast of New Zealand that is toward the west in the vicinity of Louisville. The speed of computed hot spot motion varies among models, with some models yielding almost no hot spot motion and others yielding somewhat more than 10 mm/yr. A more

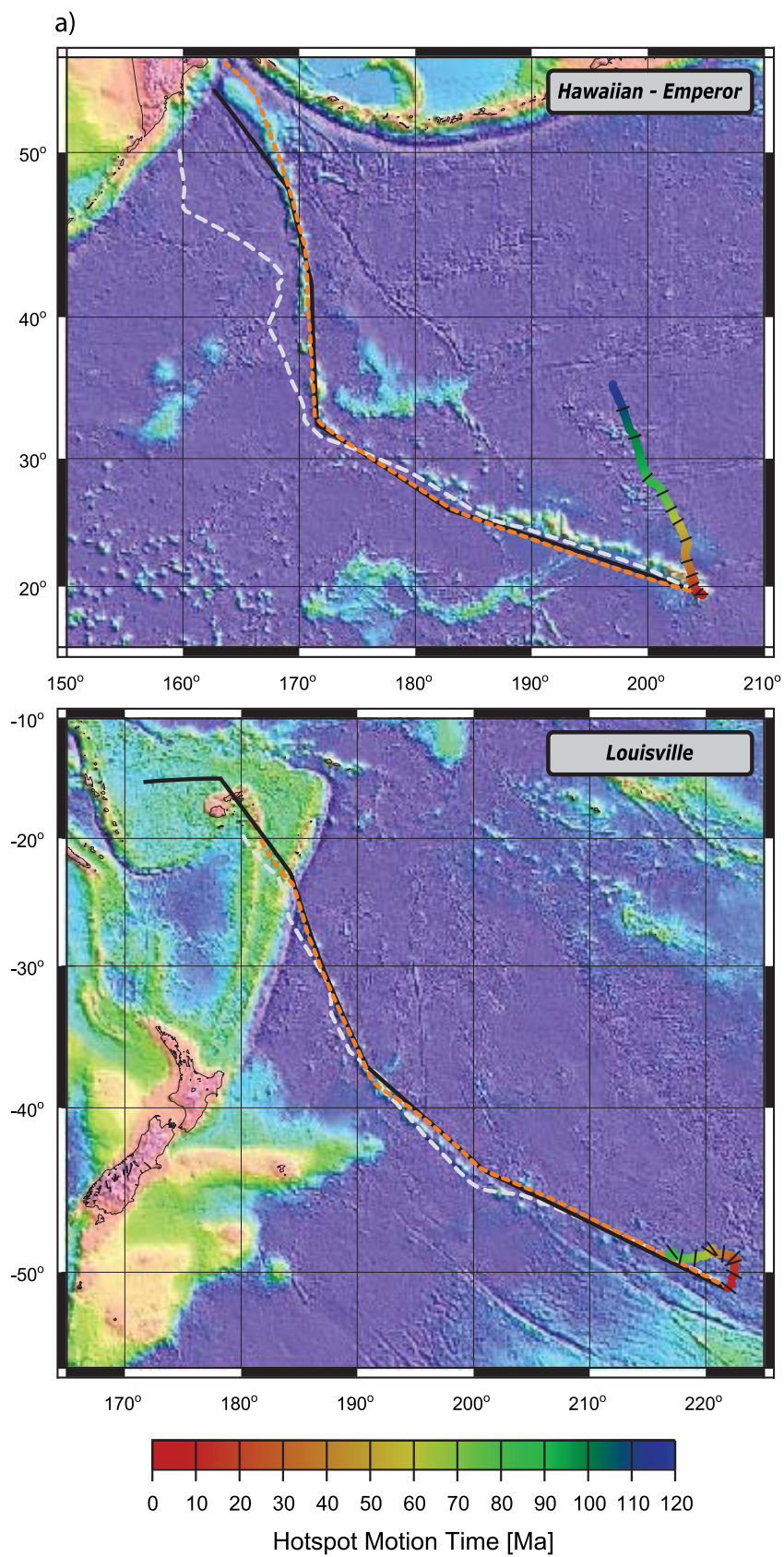


Figure 6

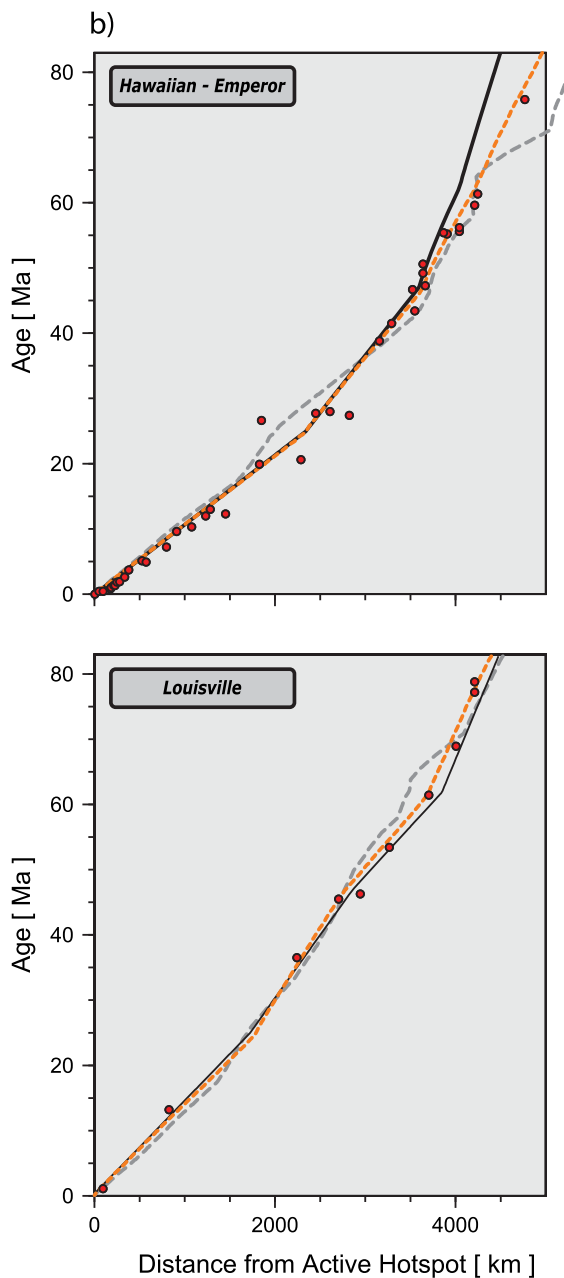


Figure 6. (continued)

detailed discussion of the results for Louisville, and comparison with the results for Hawaii, is given by *Antretter et al.* [2004]. The average of all new modeling results is quite similar to case 1 and therefore is not plotted separately.

[26] In most of these model cases the calculations show a good fit to the geometry of the seamount trails (Figure 6a), and the changes in plate rotation around 25 and 47 Ma approximately correspond to the 159°W and 169°W bends in the Louisville seamount trail (Figure 1). This holds true for models where the Hawaiian hot spot has moved southward between 83 and 47 Ma at a rate of approximately 35 mm/yr, compatible with new paleolatitude data [*Tarduno et al.*, 2003]. In the same models the Louisville hot spot has moved (south)eastward at a much slower rate, predicting a significant decrease in the distance between the two hot spots of about 1000 km from 83 to 47 Ma. Despite this remarkable inter-hot spot motion, we can fit the observed geometries and the new $^{40}\text{Ar}/^{39}\text{Ar}$ age data in both seamount trails very well.

[27] Finally, we consider plate motions and hot spot tracks globally (case 2, dashed gray lines) as done by *Steinberger et al.* [2004]. The predicted curve for the Louisville age-distance plot is still close to the data points, but the slope of the older part is smaller than the slope inferred from the actual measured ages. The predicted curve for the Hawaiian-Emperor seamount trail, however, shows a considerable misfit before 47 Ma, consistent with earlier findings [*Cande et al.*, 1995; *Raymond et al.*, 1997; *DiVenere and Kent*, 1999]. Because of the larger number of hot spot tracks being fit simultaneously, the fit to individual tracks is now not as good, but it could presumably be improved

Figure 6. Mantle flow modeling results. (a) Computed hot spot motion and tracks and (b) age-distance plots for the Hawaiian and Louisville hot spots. Hot spot motion during the past 120 Myr is shown as rainbow-colored lines as indicated by the colored scale bar; tracks and age-distance relation are shown as single-colored lines. Tick mark intervals are 10 Myr. Results are shown for the following models: Case 0, black lines: fixed hot spots with best fitting Pacific plate motion for four different rotations around the 0–25 Ma, 25–47 Ma, 47–62 Ma, and 62–83 Ma stage poles; this model assumes a plume initiation age of 120 Ma for the Louisville hot spot. Case 1, dashed orange lines: Hot spot motion computed as by *Steinberger et al.* [2004] but with a plume initiation age of 90 Ma for the Louisville hot spot; best fitting Pacific plate motion with time intervals as in case 0. Case 2, dashed gray lines: Hot spot motion as in case 1; best fit to hot spot tracks on both hemispheres, with global plate chain model 2 of *Steinberger et al.* [2004] and four rotations of the African plate with the same time intervals as in case 0.

Table A1. High-Resolution Incremental Heating Experiments

Sample Number	Sample Type	Archive Name	ERDA Hyperlink
SOTW-9-58-1a	groundmass	01C2259.zip	http://earthref.org/cgi-bin/erda.cgi?n=193
SOTW-9-58-7	groundmass	01C1919.zip	http://earthref.org/cgi-bin/erda.cgi?n=194
SOTW-9-52-1	groundmass	03C3173.zip	http://earthref.org/cgi-bin/erda.cgi?n=195
SOTW-9-48-2	groundmass	03C3213.zip	http://earthref.org/cgi-bin/erda.cgi?n=196
VM36-04	groundmass	03C3112.zip	http://earthref.org/cgi-bin/erda.cgi?n=197
VM36-03	groundmass plagioclase	03C3145.03C3276.03C3258.zip	http://earthref.org/cgi-bin/erda.cgi?n=198
VM36-02	groundmass	03C3309.03C3080.zip	http://earthref.org/cgi-bin/erda.cgi?n=199
VG-3a/MSN110-1	groundmass	01C2051.zip	http://earthref.org/cgi-bin/erda.cgi?n=200
MTHN-6D1	groundmass	01C2177.zip	http://earthref.org/cgi-bin/erda.cgi?n=201
MTHN-7D1	groundmass	01C2027.zip	http://earthref.org/cgi-bin/erda.cgi?n=202

if we allow for variations in the motion between east and west Antarctica (within geological uncertainties) in the global plate circuit. This issue will be addressed in future work.

4. Summary

[28] Following major improvements in the $^{40}\text{Ar}/^{39}\text{Ar}$ dating technique over the last decades, we successfully redated 10 samples from the *Watts et al.* [1988] study by applying high-resolution incremental heating experiments. These improved ages show that the age progression for the Louisville seamount trail is not linear after all, given that samples from the old end of this seamount trail have incremental heating $^{40}\text{Ar}/^{39}\text{Ar}$ ages that are up to 15% older than the previous ages determined by the total fusion technique. This indicates that Pacific plate motion was slower prior to 62 Ma when compared to published plate rotation models. Examination of the age progressions within the Louisville and Hawaiian-Emperor seamount trails cannot be explained by plate motion alone, but require significant motion of the hot spots themselves.

[29] In this paper we presented detailed models of mantle flow and resulting hot spot motion [cf. *Steinberger et al.*, 2004] to fit the geometries and age progressions of both the Hawaiian and Louisville hot spots. Our results indicate that the non-linear $^{40}\text{Ar}/^{39}\text{Ar}$ age progressions of the Hawaiian and Louisville hot spot tracks can be better fitted with a moving hot spot model rather than a fixed hot spot frame of reference. The same models also

indicate that the primary Hawaiian and Louisville hot spots did not move in concert, showing significant inter-hot spot motion between 80 and 47 Ma. While the Hawaiian hot spot experienced a substantial $\sim 15^\circ$ southward motion prior to 47 Ma [*Tarduno et al.*, 2003] on the basis of paleolatitude data, the Louisville hot spot is predicted to have experienced an eastward motion of $\sim 5^\circ$ during the same geological period, followed by a minor $\sim 2^\circ$ latitudinal shift over the last 30 Myr.

Appendix A: The $^{40}\text{Ar}/^{39}\text{Ar}$ Analytical Data

[30] All new $^{40}\text{Ar}/^{39}\text{Ar}$ age data reported in this study have been calculated using ArArCALC v2.2 [*Koppers*, 2002], and their resulting *.AGE files have been included in this electronic appendix. The same files also have been saved in the standard Microsoft Excel format (with the *.XLS extension) and can be opened without running ArArCALC. In Table A1 each high-resolution incremental heating experiment is listed together with its filename and a URL to download these files from the EarthRef Digital Archive (ERDA).

[31] Note that all electronic data supplements that are related to this publication can be listed online EarthRef by selecting the <http://earthref.org/cgi-bin/err.cgi?n=5002> link and by following the Quick Links. The ArArCALC v2.2 software can be directly downloaded via the <http://earthref.org/cgi-bin/erda.cgi?n=133> link, whereas the ArArCALIBRATIONS tool can be retrieved from <http://earthref.org/cgi-bin/erda.cgi?n=139>.

Acknowledgments

[32] We thank John Huard for technical support in the OSU argon dating laboratory. Financial support is provided by NSF-OCE 9730394 and NSF-OCE 0002875. Special thanks go to Hubert Staudigel, who kindly facilitated and encouraged the visits of AAPK to the OSU to perform the dating and to write this paper. We also thank John Tarduno, Dave Clague, and Warren Sharp for their thoughtful reviews.

References

- Antretter, M., P. Riisager, S. Hall, X. Zhao, and B. Steinberger (2004), Modeled paleolatitudes for the Louisville hotspot and the Ontong Java Plateau, in *Origin and Evolution of the Ontong Java Plateau*, edited by G. Fitton et al., *Geol. Soc. Spec. Publ.*, in press.
- Cande, S. C., and D. V. Kent (1995), Revised calibration of the geomagnetic polarity timescale for the late Cretaceous and Cenozoic, *J. Geophys. Res.*, *100*(B4), 6093–6095.
- Cande, S. C., C. A. Raymond, J. Stock, and W. F. Haxby (1995), Geophysics of the Pitman Fracture Zone and Pacific-Antarctic plate motions during the Cenozoic, *Science*, *270*(5238), 947–953.
- Courtillot, V., A. Davaille, J. Besse, and J. Stock (2003), Three distinct types of hotspots in the Earth's mantle, *Earth Planet. Sci. Lett.*, *205*(3–4), 295–308.
- Dalrymple, G. B., E. C. Alexander, M. A. Lanphere, and G. P. Kraker (1981), Irradiation of samples for ⁴⁰Ar/³⁹Ar dating using the Geological Survey TRIGA reactor, *U.S. Geol. Surv. Prof. Pap.*, *1176*, 55 pp.
- DiVenere, V., and D. V. Kent (1999), Are the Pacific and Indo-Antarctic hotspots fixed? Testing the plate circuit through Antarctica, *Earth Planet. Sci. Lett.*, *170*(1–2), 105–117.
- Duncan, R. A., and D. A. Clague (1985), Pacific plate motion recorded by linear volcanic chains, in *The Ocean Basins and Margins*, vol. 7A, *The Pacific Ocean*, edited by A. E. A. Nairn, F. L. Stehli, and S. Uyeda, pp. 89–121, Plenum, New York.
- Duncan, R. A., and M. A. Richards (1991), Hotspots, mantle plumes, flood basalts, and true polar wander, *Rev. Geophys.*, *29*, 31–50.
- Fleck, R. J., J. F. Sutter, and D. H. Elliot (1977), Interpretation of discordant ⁴⁰Ar/³⁹Ar age-spectra of Mesozoic tholeiites from Antarctica, *Geochim. Cosmochim. Acta*, *41*, 15–32.
- Foulger, G. R., and J. H. Natland (2003), Is “hotspot” volcanism a consequence of plate tectonics?, *Science*, *300*(5621), 921–922.
- Hawkins, J. W., P. F. Lonsdale, and R. Batiza (1987), Petrologic evolution of the Louisville seamount chain, in *Seamounts, Islands, and Atolls*, *Geophys. Monogr. Ser.*, vol. 43, edited by B. H. Keating et al., pp. 235–254, AGU, Washington, D. C.
- Keller, R. A., R. A. Duncan, and M. R. Fisk (1995), Geochemistry and ⁴⁰Ar/³⁹Ar geochronology of basalts from ODP Leg 145, *Proc. Ocean Drill. Program Sci. Results*, *145*, 333–344.
- Koppers, A. A. P. (2002), ArArCALC—Software for Ar-40/Ar-39 age calculations, *Comput. Geosci.*, *28*(5), 605–619.
- Koppers, A. A. P., H. Staudigel, J. R. Wijbrans, and M. S. Pringle (1998), The Magellan seamount trail: Implications for Cretaceous hotspot volcanism and absolute Pacific plate motion, *Earth Planet. Sci. Lett.*, *163*(1–4), 53–68.
- Koppers, A. A. P., H. Staudigel, and J. R. Wijbrans (2000), Dating crystalline groundmass separates of altered Cretaceous seamount basalts by the Ar-40/Ar-39 incremental heating technique, *Chem. Geol.*, *166*(1–2), 139–158.
- Koppers, A. A. P., J. P. Morgan, J. W. Morgan, and H. Staudigel (2001), Testing the fixed hotspot hypothesis using Ar-40/Ar-39 age progressions along seamount trails, *Earth Planet. Sci. Lett.*, *185*(3–4), 237–252.
- Koppers, A. A. P., H. Staudigel, and R. A. Duncan (2003a), High-resolution ⁴⁰Ar/³⁹Ar dating of the oldest oceanic basement basalts in the western Pacific basin, *Geochem. Geophys. Geosyst.*, *4*(11), 8914, doi:10.1029/2003GC000574.
- Koppers, A. A. P., H. Staudigel, M. S. Pringle, and J. R. Wijbrans (2003b), Short-lived and discontinuous intraplate volcanism in the South Pacific: Hot spots or extensional volcanism?, *Geochem. Geophys. Geosyst.*, *4*(10), 1089, doi:10.1029/2003GC000533.
- Kullerud, L. (1991), On the calculation of isochrones, *Chem. Geol.*, *87*, 115–124.
- Lonsdale, P. (1988), Geography and history of the Louisville hotspot chain in the Southwest Pacific, *J. Geophys. Res.*, *93*, 3078–3104.
- Mahoney, J. J., M. Storey, R. A. Duncan, K. J. Spencer, and M. S. Pringle (1993), Geochemistry and age of the Ontong Java Plateau, in *The Mesozoic Pacific: Geology, Tectonics, and Volcanism*, *Geophys. Monogr. Ser.*, vol. 77, edited by M. S. Pringle et al., pp. 233–261, AGU, Washington, D. C.
- McDougall, I., and T. M. Harrison (1988), *Geochronology and Thermochronology by the ⁴⁰Ar/³⁹Ar Method*, 212 pp., Oxford Univ. Press, New York.
- Min, K. W., R. Mundil, P. R. Renne, and K. R. Ludwig (2000), A test for systematic errors in Ar-40/Ar-39 geochronology through comparison with U/Pb analysis of a 1.1-Ga rhyolite, *Geochim. Cosmochim. Acta*, *64*(1), 73–98.
- Morgan, W. J. (1972), Plate motions and deep mantle convection, *Mem. Geol. Soc. Am.*, *132*, 7–122.
- Neal, C. R., J. J. Mahoney, L. W. Kroenke, R. A. Duncan, and M. G. Pettersson (1997), The Ontong Java Plateau, in *Large Igneous Provinces: Continental, Oceanic, and Planetary Flood Volcanism*, *Geophys. Monogr. Ser.*, vol. 100, edited by J. J. Mahoney and M. Coffin, pp. 183–216, AGU, Washington, D. C.
- Pringle, M. S. (1993), Age progressive volcanism in the Musicians Seamounts: A test of the hot spot hypothesis for the late Cretaceous Pacific, *The Mesozoic Pacific: Geology, Tectonics, and Volcanism*, *Geophys. Monogr. Ser.*, vol. 77, edited by M. S. Pringle et al., pp. 187–216, AGU, Washington, D. C.
- Raymond, C. A., J. M. Stock, and S. C. Cande (1997), Relative hotspot motion based on global plate reconstructions, paper presented at Chapman Conference on the History and Dynamics of Global Plate Motions, AGU, Marshall, Calif.

- Renne, P. R., A. L. Deino, R. C. Walter, B. D. Turrin, C. C. Swisher III, T. A. Becker, G. H. Curtis, W. D. Sharp, and A.-R. Jaouni (1994), Intercalibration of astronomical and radioisotopic time, *Geology*, *22*, 783–786.
- Renne, P. R., C. C. Swisher, A. L. Deino, D. B. Karner, T. L. Owens, and D. J. DePaolo (1998), Intercalibration of standards, absolute ages and uncertainties in $^{40}\text{Ar}/^{39}\text{Ar}$ dating, *Chem. Geol.*, *145*, 117–152.
- Roddick, J. C. (1978), The application of isochron diagrams in $^{40}\text{Ar}-^{39}\text{Ar}$ dating: A discussion, *Earth Planet. Sci. Lett.*, *41*, 233–244.
- Sharp, W. D., and D. A. Clague (2002), An older, slower Hawaii-Emperor bend, *Eos Trans. AGU*, *83*(47), Fall Meet. Suppl., Abstract T61C-04.
- Smith, A. D., and C. Lewis (1999), Differential rotation of lithosphere and mantle and the driving forces of plate tectonics, *J. Geodyn.*, *28*(2–3), 97–116.
- Steiger, R. H., and E. Jäger (1977), Subcommittee on geochronology: Convention on the use of decay constants in geo- and cosmochronology, *Earth Planet. Sci. Lett.*, *36*, 359–362.
- Steinberger, B. (2000), Plumes in a convecting mantle: Models and observations for individual hotspots, *J. Geophys. Res.*, *105*(B5), 1127–1152.
- Steinberger, B., and R. J. O’Connell (1998), Advection of plumes in mantle flow: Implications for hotspot motion, mantle viscosity and plume distribution, *Geophys. J. Int.*, *132*(2), 412–434.
- Steinberger, B., R. Sutherland, and R. J. O’Connell (2004), Mantle flow models constrained by revised global plate motions successfully predict the Emperor-Hawaii and other hotspot-related seamount chains, *Nature*, in press.
- Tarduno, J. A., et al. (2003), The Emperor Seamounts: Southward motion of the Hawaiian hotspot plume in Earth’s mantle, *Science*, *301*, 1064–1069.
- Taylor, J. R. (1997), *An Introduction to Error Analysis*, 327 pp., Univ. Sci. Books, Mill Valley, Calif.
- Tejada, M. L. G., J. J. Mahoney, R. A. Duncan, and M. P. Hawkins (1996), Age and geochemistry of basement and alkalic rocks of Malaita and Santa Isabel, Solomon Islands, southern margin of Ontong Java plateau, *J. Petrol.*, *37*(2), 361–394.
- Watts, A. B., J. K. Weisell, R. A. Duncan, and R. L. Larson (1988), Origin of the Louisville Ridge and its relationship to the Eltanin fracture zone system, *J. Geophys. Res.*, *93*, 3051–3077.
- Wessel, P., and L. Kroenke (1997), A geometric technique for relocating hotspots and refining absolute plate motions, *Nature*, *387*, 365–369.
- York, D. (1969), Least squares fitting of a straight line with correlated errors, *Earth Planet. Sci. Lett.*, *5*, 320–324.